IEEE Photonics Journal
An IEEE Photonics Society Publication

Open Access

Optical Trapping and Separation of Metal Nanoparticles by Cylindrical Metalenses With Phase Gradients

Volume 12, Number 4, August 2020

Zhe Shen
Ziyao Wang
Hongchao Liu
Yaochun Shen

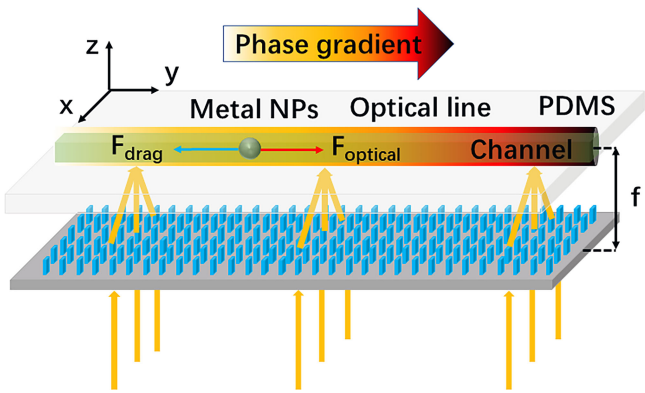

DOI: 10.1109/JPHOT.2020.3005944

Optical Trapping and Separation of Metal Nanoparticles by Cylindrical Metalenses With Phase Gradients

Zhe Shen,[1] **Ziyao Wang**,[1] **Hongchao Liu**,[2] **and Yaochun Shen**[3]

[1]School of Electronic and Optical Engineering, Nanjing University of Science and Technology, Nanjing 210094, China
[2]Joint Key Laboratory of the Ministry of Education, Institute of Applied Physics and Materials Engineering, University of Macau, Avenida da Universidade, Taipa 999078, China
[3]Department of Electrical Engineering & Electronics, University of Liverpool, Liverpool L69 3GJ, U.K.

DOI:10.1109/JPHOT.2020.3005944

Manuscript received May 5, 2020; revised June 9, 2020; accepted June 25, 2020. Date of publication June 30, 2020; date of current version July 14, 2020. This work was supported in part by the National Natural Science Foundation of China (NSFC) under Grant 61805119 in part by the Natural Science Foundation of Jiangsu Province under Grant BK20180469 in part by the Fundamental Research Funds for the Central Universities (30919011275), and in part by the Start-up Research Grant of University of Macau (SRG2019-00174-IAPME). Corresponding author: Zhe Shen (e-mail: shenzhe@njust.edu.cn)

Abstract: We proposed a method for driving metal nanoparticles in the focal field by cylindrical metalens with phase gradient. It was found that the introduced gradient phase would not affect the formation of the focal line, where metal nanoparticles can be trapped. While being driven along the direction with the phase gradient, Ag nanoparticles with different sizes, and nanoparticles with different materials (Au and Ag) were successfully separated, respectively. The induced driving force has an approximately linear relationship with the phase gradient. This kind of planar thin structure can be combined with a microfluidic chip to form a miniaturized system for label-free and non-contact sorting of particles or biological cells, and it may find potential applications in biomedicine.

Index Terms: Optical trapping, optical sorting, metal nanoparticles, metalens, phase gradient.

1. Introduction

Sorting particles or biological cells plays an important role in colloidal physics, analytical chemistry, and biomedicine. The miniaturization of the sorting system is a tendency for integrated and portable applications. Based on lab-on-a-chip, several microfluidic methods including fluorescence-activated cell sorters [1], electrodynamics mobilization of fluid [2], dielectrophoretic forces [3], and hydrodynamic flow control [4] have been developed. However, fluorescent labels, microfluidic buffers, and electrophoretic damage can either contaminate the sample or affect the result. Therefore, there is a need to develop label-free and non-invasive methods for particle sorting.

In 1986, Ashkin and his colleagues invented optical tweezers for particle trapping by creating a three-dimensional (3D) potential well through a highly focused laser with an objective lens [5]. The focal field can selectively deflect running particles in solution. That is, when two groups of particles flow through the focal field, after the competition between optical force and fluid force, one group of particles deviates from the original direction of motion, while the other group of particles continues

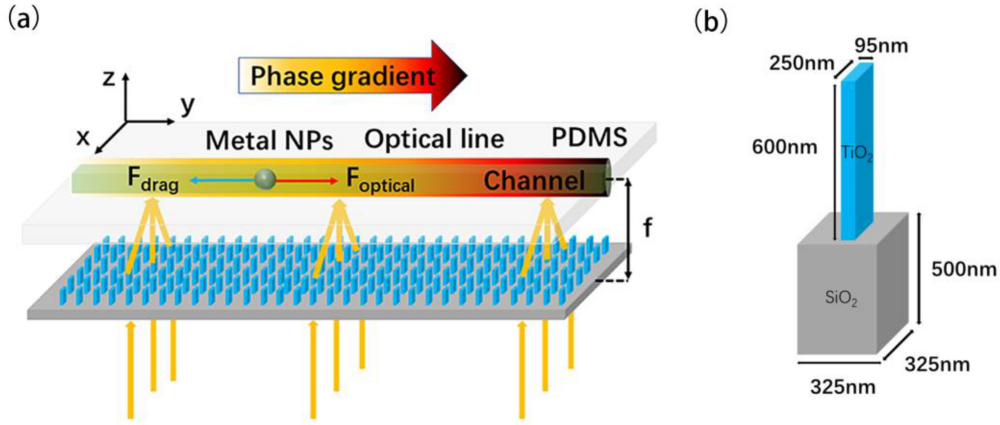

Fig. 1. (a) The schematic of the particle manipulation system based on a cylindrical metalens with phase gradient. (b) The metalens unit cell that consists of a TiO_2 nanofin and a SiO_2 substrate.

flowing without influence. The separation is determined by the inherent properties of particles such as sizes or refractive indices. Due to its non-contact form, this method has been intensively used for optical sorting [6]–[8]. For large-area sorting, several devices including microlens array [7], [9], [10], diffraction optical element [11], and spatial light modulator [12], [13] have been utilized to generate optical lattice for sorting in the last decade. However, these structures are bulky, expensive, and not easy to be integrated. Configurations of waveguide and thin metal film can overcome these limitations with driving particles through surface waves of evanescent wave [14] and surface plasmon wave [15], respectively, and they were potentially used for sorting particles [16], [17]. Nevertheless, they have high scattering and absorption losses, and the operations are only confined at their surfaces within limited ranges.

In recent years, metasurfaces have been considered to be promising two-dimensional meta-materials with various geometries, which impart phase for controlling phase, amplitude, and polarization of transmitted or reflected electromagnetic waves in a desired and flexible manner [18]–[22]. Because of the freedom for wavefront control, metasurfaces have been manufactured to be lenses [23]–[25], waveplates [26]–[28], polarizers [29]–[33], and so on. Metalens as an alternative of the objective lens was used for laser focusing [23] and further applied for optical trapping [34]. The trapping of nanoparticles was numerically achieved with optical vortex array generated by a multifocal metalens [24]. Selective trapping of metal particles was demonstrated by polarization-sensitive metalens [35], [36]. Metalens is also easily engineered with phase gradients [37]. In the form of scattering forces, optical forces arising from the phase gradients in extended laser beams to drive particles [38], [39] provide a new possibility for particle manipulation, which can be combined with microfluidics for particle sorting.

In this work, a method was proposed for optical trapping and separation of metal nanoparticles by using cylindrical metalens with phase gradient. Particles with different sizes or materials were examined. Finite-difference time-domain (FDTD) method was used to calculate the optical forces and potentials of particles in the focal fields. The simulation results show that the particles can be laterally trapped and longitudinally driven.

2. Method and Theory

2.1 The Metalens Structure

As shown in Fig. 1(a), through a metalens, normally incident light is focused to the channel in the polydimethylsiloxane (PDMS), where a metal nanoparticle is trapped. Through adding a phase gradient in the *y*-direction, the particle experiences optical force to compensate drag force. Fig. 1(b)

shows the unit cell of the metalens, which is composed of a titanium dioxide (TiO_2) nanofin and a silica (SiO_2) substrate. By choosing the nanofin with length, width, and thickness of 250 nm, 95 nm, and 600 nm, respectively, it is designed to be a half waveplate at the working wavelength of 740 nm. The length, width, and thickness of the substrate are 325 nm, 325 nm, and 500 nm, respectively. The center-to-center spacing of the nanofins is 325 nm. The material TiO_2 is lossless and its refractive index is high in the visible regime. For high-index dielectric metasurfaces, the interaction among the nanofins is negligible and light scattered at each nanofin is dominated with the local waveguide effect. Thus, the transmission coefficient of the unit cell array can be roughly seen as an individual response of a unit cell [40], [41], which maintains transmission efficiency as high as 90% according to Ref. [24].

These transparent nanofins have resonant behaviors and allow for manipulating the phase of locally transmitted light over the whole 2π range through precise engineering in two dimensions. Due to the birefringence, the effective refractive indices of nanofins vary for two orthogonal polarizations perpendicular to the propagation direction. For incident right-handed circularly polarized light, the phase change and rotation angle of a nanofin have a relationship: $\varphi_{nf}(x, y) = 2\theta_{nf}(x, y)$, according to the Pancharatnam-Berry (PB) phase [42], [43]. The phase and angle profiles of nanofins in a focusing metalens should satisfy [23]

$$\varphi_{nf}(x, y) = \frac{2\pi}{\lambda_d}\left(f - \sqrt{x^2 + y^2 + f^2}\right), \tag{1}$$

$$\theta_{nf}(x, y) = \frac{\pi}{\lambda_d}\left(f - \sqrt{x^2 + y^2 + f^2}\right), \tag{2}$$

where λ_d is the wavelength, f is the focal length.

2.2 Optical Force, Trapping Potential and Drag Force

The time-averaged optical force applied to a particle can be calculated through the integral of Maxwell stress tensor (MST) on the particle surface [24].

$$< F > = \int \left\{\frac{\varepsilon}{2}\mathrm{Re}[(E \cdot n)E^*] - \frac{\varepsilon}{4}(E \cdot E^*)n + \frac{\mu}{2}\mathrm{Re}[\mu(H \cdot n)H^*] - \frac{\mu}{4}(H \cdot H^*)n\right\} ds, \tag{3}$$

where ε and μ are the relative dielectric constant and magnetic permeability of the medium surrounding the particle, n is the normal unit perpendicular to the integral area s. The optical force can be obtained by the MST toolbox available in a commercial solver (FDTD solutions, Lumerical). Note that the total force is composed of the gradient force and scattering force.

The trapping potential can be calculated by the following formula [44]:

$$U(r_0) = -\int_{\infty}^{r_0} F(r) dr, \tag{4}$$

where $U(r_0)$ is the energy required to move a particle from infinity to position r_0. To obtain a stable trap, a trapping potential depth of more than $10k_BT$ is generally required to overcome the interference from thermal effect [45], where k_B the Boltzmann constant and T is the temperature.

One-dimensional Langevin equation can be used to describe the linear motion of a trapped particle. Assuming that the motion is at the overdamped limit, the acceleration is negligible in a short distance, and the noise is ignored, the equation can be simplified as

$$\gamma \frac{dy}{dt} = F(y), \tag{5}$$

where y is the position of the particle, $F(y)$ is the optical force exerted the particle at the position y, and γ is the friction coefficient, which is defined by Stokes' law, $\gamma = 6\pi\upsilon R$, where R is the radius of the particle and υ is the dynamic viscosity of the medium.

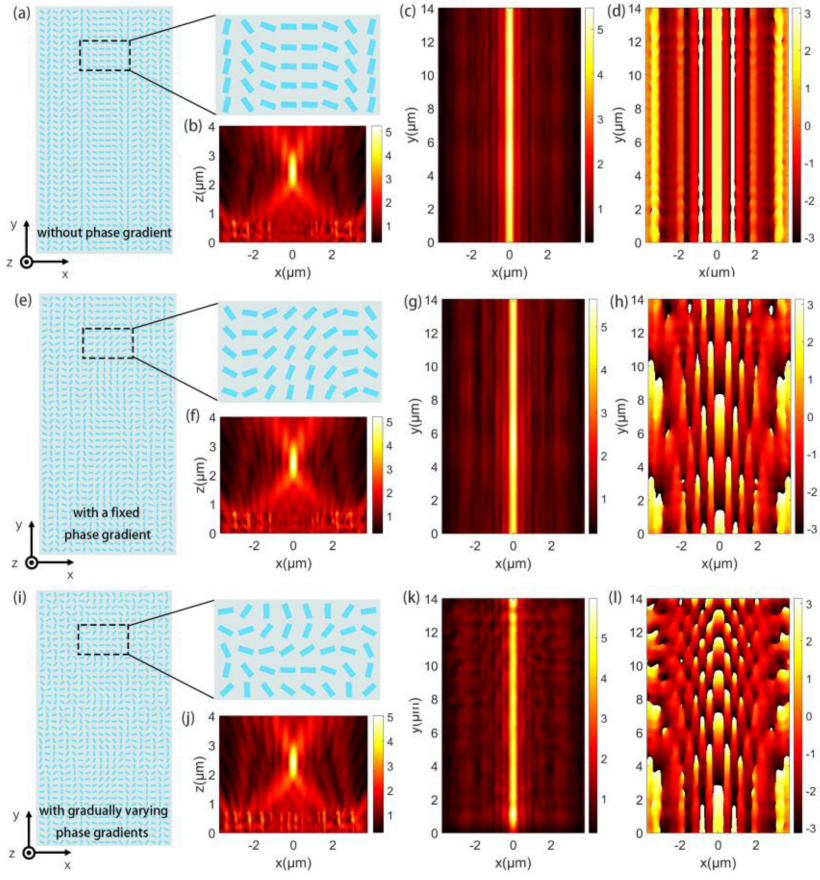

Fig. 2. (a), (e), and (i) Top views of cylindrical metalenses without phase gradient, with a fixed phase gradient, and with gradually varying phase gradients, respectively. The right pics show the enlargements of partial metalens structures. (b), (f), and (j) The corresponding electrical intensities in the propagation *x*-*z* planes. The interface between nanofin and substrate is at $z = 0$ μm. (c), (g), and (k) The corresponding electrical intensities in the focal *x*-*y* planes. (d), (h), and (l) The corresponding E_y phase distributions in the focal *x*-*y* planes.

3. Results and Discussions

3.1 The Cylindrical Metalens

To design a cylindrical metalens without phase gradient, the phase changes and rotation angles of the metalens nanofins need to follow [46]

$$\varphi_{nf}(x, y) = \frac{2\pi}{\lambda_d}\left(f - \sqrt{x^2 + f^2}\right), \tag{6}$$

$$\theta_{nf}(x, y) = \frac{\pi}{\lambda_d}\left(f - \sqrt{x^2 + f^2}\right). \tag{7}$$

As shown in Fig. 2(a), the nanofins in the cylindrical metalens without phase gradient are continuous in the *y*-direction, and the rotation angles of the nanofins far from the middle change more rapidly than those close to the middle. To facilitate simulation calculations, the metalenses were designed with a focal length of 2 μm and a size of 7×14 μm^2, including 20 columns and 40 rows. It is worth mentioning that the number of unit cells or the size of the metasurface can also influence the performance of the device. Note that our suggested design concept is not the only possible implementation that can meet the specified conditions. However, due to its inherent

simplicity that all the constituent unit cells are identical in shape and size, our solution offers great ease for experimental realization.

To design a cylindrical metalens with phase gradient in the *y*-direction, the phase changes and rotation angles of the metalens nanofins need to follow

$$\varphi_{nf}(x, y) = \frac{2\pi}{\lambda_d}\left(f - \sqrt{x^2 + f^2}\right) + \frac{2\pi}{ad}y^b, \tag{8}$$

$$\theta_{nf}(x, y) = \frac{\pi}{\lambda_d}\left(f - \sqrt{x^2 + f^2}\right) + \frac{\pi}{ad}y^b, \tag{9}$$

where a and b are the factors of the phase gradient, and d is the center-to-center spacing of the nanofins. As shown in Fig. 2(e), the rotation angles of nanofins increase by the step size of $\pi/20$ per row in the *y*-direction. A total rotation angle change of 2π was added to the *y*-direction for a phase gradient of $\pi/20d$ (rad/m). In this case, $a = 20$ and $b = 1$. The bottom row of nanofins is the same in all cases for reference. As shown in Fig. 2(i), the rotation angles of nanofins each row increase nonlinearly from bottom to top, the phase gradients are gradually varying. In this case, $a = 320$ and $b = 2$.

The focal fields by the three metalenses above were simulated. The collimated light normally illuminates from the beneath of the substrate, across the nanofins, to the air. Then, the corresponding far-field distribution was obtained by a field monitor. For the metalenses in Figs. 2(a) and (e), periodic boundary conditions were used in the *y*-direction while perfect matching layer (PML) boundaries were used in the *x*- and *z*- directions. For the metalens in Fig. 2(k), the periodic boundary condition is not applicable in *y*-direction due to nonuniform structure distribution, all the boundary conditions were using PMLs. The mesh step of the simulations was 5 nm. Figs. 2(b), (f), and (j) are the calculated light intensity distributions in the *x*-*z* plane, showing the convergence behaviors. The focal points are all located at about $z = 1.9$ μm, which is slightly different from the designed focal length. This is consistent with Eqs. (8) and (9) that the focal length f is independent of the position *y*. Figs. 2(c), (g), and (k) are the calculated light intensity distributions in the focal *x*-*y* planes. Clear focal lines at the middle ($x = 0$ μm) can be seen, indicating the introduced phase gradient has almost no effect on the focusing by the phase changes in the *x*-direction. Because of the different boundary conditions applied in simulation, the distribution in Fig. 2(k) is slightly different from the other two. With the introduction of relatively large phase gradient, the rotation angle distribution changes significantly. As the transmission efficiency of nanofin with different angles differs, thus the intensity at the focal line in Fig. 2(k) is slightly nonuniform. Figs. 2(d), (h), and (l) are the calculated phase distributions in the focal *x*-*y* plane. Phase responses were obtained by extracting the transmission electrical field components and calculating $\arctan[\mathrm{Im}(E_y)/\mathrm{Re}(E_y)]$. It can be seen from Fig. 2(h) that there is a 4π phase change in the *y*-direction, which is particularly clear in the middle, while the phase distribution in Fig. 2(d) remains uniform in the *y*-direction. In Fig. 2(l), it can be seen in the middle that the phase gradients increase from bottom to top. All the phase distributions are in good consistency with the designs for all the metalenses. Therefore, the phase gradient of the cylindrical metalens can be independently controlled by adjusting the values of a and b, offering great freedom degree.

3.2 Optical Trapping of Metal Nanoparticles by a Cylindrical Metalens With a Fixed Phase Gradient

By using the metalens in Fig. 2(e), we studied the trapping of Ag nanoparticles with radii every 50 nm from 50 nm to 400 nm. In the simulation, the power of the incident light was 0.98 mW, the medium around Ag nanoparticles was water ($n_s = 1.33$), which was not embedded around the nanofins for practical consideration. Both the sample and metalens can be adjusted freely in 3D directions, this avoids the contamination of metalens and offers great freedom for optical adjustment and alignment. Then we calculated the trapping forces and potential depths for Ag nanoparticles with different sizes according to Eqs. (3) and (4). It can be seen from Fig. 3(a), when the radii are less than 200 nm, Ag nanoparticles are subjected to forces that always point to the zero point at

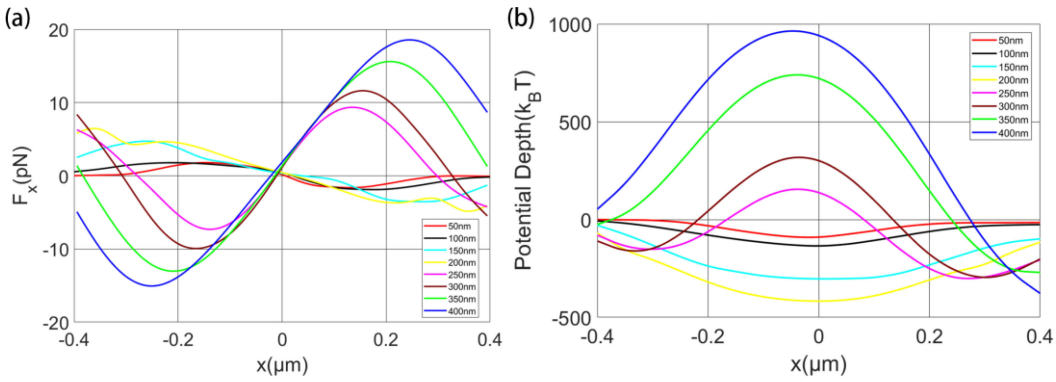

Fig. 3. (a) Relationships between F_x and the position at the x-axis ($y = 0$) of Ag nanoparticles. (b) Relationships between the potential depth and the position at the x-axis ($y = 0$) of Ag nanoparticles. The inserts in (a) and (b) indicate the radii of the particles.

the x-axis. This is because plasmonic nanoparticles can be trapped due to the localized surface plasmon resonance [47] whilst large particles cannot. This can also be explained by the competition between gradient force (pulling) and scattering force (pushing). When the radii of Ag nanoparticles are larger than 200 nm, the directions of forces are opposite, and traps cannot be formed. When the size of a particle is relatively small, the particle is easily polarized, the gradient force(Coulomb force) from the intensity gradient is dominant that points to the middle with higher intensity. While when the size of a particle is relatively large, the x-direction component of the scattering force can be dominant that points to two sides with lower intensity. As shown in Fig. 3(b), when the radii of Ag nanoparticles are smaller than 200 nm, potential wells can be generated. When the radii of Ag nanoparticles are at the range 50 nm$\sim$200 nm, the potential depths are larger than $10k_BT$, stable traps can be obtained.

3.3 Optical Separation of Metal Nanoparticles by a Cylindrical Metalens With a Fixed Phase Gradient

Based on the trapping of metal nanoparticles by the cylindrical metalens with a fixed phase gradient, we firstly studied the effect of the size on the force of metal nanoparticles. Among the trapped Ag nanoparticles above, those with radii of 50 nm and 100 nm were selected as the simulation objects. Under the conditions of stable traps as illustrated in Figs. 4(a) and (b), the phase gradient forces of Ag nanoparticles with these two radii were studied. We measured F_y every 1 μm from -5 μm to 5 μm in the y-direction ($x = 0$), as shown in Fig. 4(c). F_y of Ag nanoparticles with the two different sizes are separately distributed in two regions. The average F_y value of Ag nanoparticles with a radius of 50 nm is 0.325 pN, and that of Ag nanoparticles with a radius of 100 nm is 2.16 pN. With the phase gradient forces, metal nanoparticles can be driven along the focal line, which can be regarded as a nano-optical conveyor belt for transporting particles or biological cells.

In order to study the behaviors of Ag nanoparticles in the focal field, we used Eq. (5) to calculate the instantaneous velocity $v = dy/dt$ of Ag nanoparticles at various positions. As shown in Fig. 4(d), the velocity values of Ag nanoparticles with two radii are separately distributed in two regions. The velocity values of Ag nanoparticles with a radius of 50 nm are all around 0.3 μm/s, while that of 100 nm are all around 1.5 μm/s. Fig. 4(e) shows the time required for Ag nanoparticles with two radii to move from the current position to the next position. The instantaneous velocity of the particle at each position was taken as the average velocity at 1 μm interval between two positions. It takes 23.307 s for a Ag nanoparticle with a radius of 50 nm to travel through the whole focal line, while it takes only 3.341 s for a Ag nanoparticle with a radius of 100 nm. These results demonstrate that metal nanoparticles of different sizes can be separated by the phase gradient metalens.

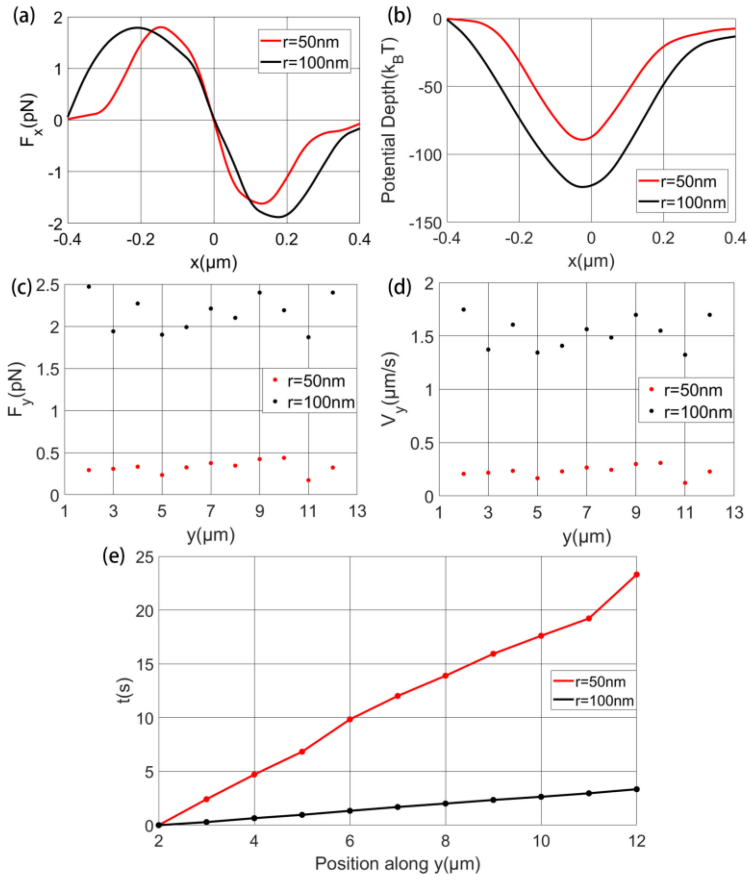

Fig. 4. (a) Relationships between F_x and the position at the x-axis ($y = 0$), (b) potential depth distributions along x-direction, and (c), (d), and (e) scatter plots of $F_y - y$, $V_y - y$, and t-y ($x = 0$), for Ag nanoparticles with radii of 50 nm and 100 nm, respectively.

Secondly, we studied the effect of the material on the force of nanoparticles. Ag and Au nanoparticles with the same radius of 75 nm were chosen as the simulation objects. The magnitude of the trapping force F_x is at the level of pN. The potential depths are greater than $10k_BT$. Both Ag and Au nanoparticles can be stably trapped at the focal line. As shown in Fig. 5(c), the average F_y of Au and Ag nanoparticles are respectively 1.91 pN and 1.70 pN, respectively. The fluctuation of the forces comes from the variation of the laser intensity in the y-axis, as the intensity gradient force (gradient force) will cause changes to the phase gradient force (scattering force). Then we calculated the instantaneous velocities of Au and Ag nanoparticles at each position according to Eq. (5), as shown in Fig. 5(d). Next, we calculated the time required for the two groups of nanoparticles to move from the current position to the next position, as shown in Fig. 5(e). It takes 3.784 s for Au nanoparticle with a radius of 75 nm to move through the focal line, while it takes 4.613 s for Ag nanoparticle. These results demonstrate that nanoparticles with different materials can be separated by the phase gradient metalens.

3.4 The Phase Gradient Dependent Force

Finally, we studied the effect of the phase gradient on the force of metal nanoparticles. By modulating the factors a and b in Eq. (8), the phase gradient in the y-direction can be adjusted. Here, we chose $b = 1$ and $a = 3, 4, 6, 10, 20, 40, 80, 120$ respectively for the design of the metalenses. The maximum phase gradient is $\pi/3d$ (rad/m), which is formed by at least three rows of nanofins. We got a boxplot for F_y of Ag nanoparticles with a radius of 100 nm in the y-direction

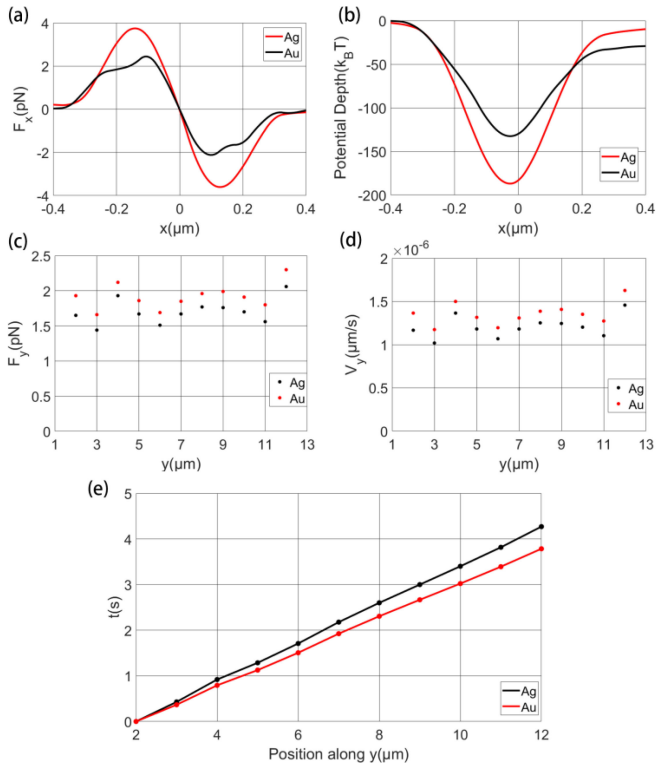

Fig. 5. (a) Relationships between F_x and the position at the x-axis ($y = 0$), (b) potential depth distributions, and (c), (d), and (e) scatter plots of $F_y - y$, $V_y - y$, and t-y ($x = 0$), for Ag and Au nanoparticles with the same radius of 75 nm, respectively.

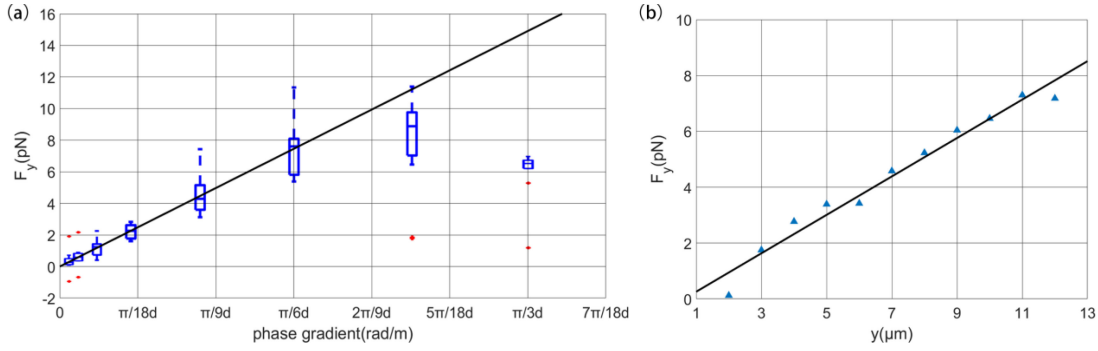

Fig. 6. (a) Boxplot of F_y in the y-direction ($x = 0$) for Ag nanoparticles with a radius of 100 nm under phase gradients with π/120d, π/80d, π/40d, π/20d, π/10d, π/6d, π/4d, and π/3d (*rad/m*). The blue dotted lines indicate the ranges of the force values, the blue boxes indicate the quartiles, the lines in the boxes indicate the median values, and the red dots indicate the outliers. The black inclined line is fitted based on the median values excluding those at $\pi/3d$ and $\pi/4d$ by using the least square method. (b) Scatter plots of $F_y - y$ of a Ag nanoparticle with a radius of 100 nm in the y-direction ($x = 0$). The black line is fitted by using the least square method. The abscissa denotes the position of the particle located at the focal line by the metalens in Fig. 2(i).

($x = 0$) under different phase gradients, as shown in Fig. 6(a). The force has an approximately linear relationship with the phase gradient when it is less than $\pi/6d$ (rad/m). As for the relatively large phase gradients of $\pi/3d$ or $\pi/4d$ (rad/m), the focal field may be affected because the phase changes drastically, as shown in Fig. 2(k), thus the force deviates from the ideal value. The situation for the case of $\pi/3d$ is worse, thus the average force is lower than that of $\pi/4d$. The negative values

of the forces in the *y*-direction can be attributed to that the phase gradient forces are too small to overcome the gradient forces.

In order to study the effect of forces by the nonuniform phase gradients, we further measured F_y of a Ag nanoparticle with a radius of 100 nm at the focal line by the metalens in Fig. 2(i). The metalens has linearly increasing phase gradients with the quadratic phase profile. As shown in Fig. 6(b), along with the phase gradient increasing from bottom to top, the force F_y of the Ag nanoparticle increases. Since the phase gradients are relatively small, the forces and phase gradients still maintain an approximately linear relationship. Therefore, different phase gradients can be imprinted on a single metalens for dynamic manipulation of particles.

4. Conclusion

In summary, we numerically studied cylindrical metalenses without and with phase gradients, the former can be potentially used for particle self-assembly with a line trap, the latter can be used for driving particles along the direction with phase gradient, which can be further used for optical separation of metal nanoparticles with different sizes or materials. The driving forces on metal nanoparticles have a linear relationship with relatively small phase gradients. Compared with traditional optical trapping by objective, cylindrical metalenses with phase gradients can be used to move particles without the need of any mechanical movement. Compared with previous methods of driving particles through surface waves including evanescent wave or surface plasmon wave, the phase gradient focal field can be constructed in the 3D space rather than on the surface only, thus avoiding physical contact between particle solution and structure. This manipulation mechanism can be cooperated with microfluidics to achieve more controlled particle sorting. This work may open up new avenues for optical tweezers and their application in biomedicine.

Acknowledgment

The authors would like to thank the anonymous reviewers for their valuable suggestions.

References

[1] W. A. Bonner, H. R. Hulett, R. G. Sweet, and L. A. Herzenberg, "Fluorescence activated cell sorting," *Rev. Sci. Instrum.*, vol. 43, no. 3, pp. 404–409, Mar. 1972.
[2] A. Y. Fu, C. Spence, A. Scherer, F. H. Arnold, and S. R. Quake, "A microfabricated fluorescence-activated cell sorter," *Nat. Biotechnol.*, vol. 17, no. 11, pp. 1109–1111, Nov. 1999.
[3] S. Fiedler, S. G. Shirley, T. Schnelle, and G. Fuhr, "Dielectrophoretic sorting of particles and cells in a microsystem," *Anal. Chem.* vol. 70, no. 9, pp. 1909–1915, May 1998.
[4] A. Wolff *et al.*, "Integrating advanced functionality in a microfabricated high-throughput fluorescent-activated cell sorter," *Lab Chip*, vol. 3, no. 1, pp. 22–27, Feb. 2003.
[5] A. Ashkin, J. M. Dziedzic, J. E. Bjorkholm, and S. Chu, "Observation of a single-beam gradient force optical trap for dielectric particles," *Opt. Lett.*, vol. 11, no. 5, pp. 288–290, May 1986.
[6] R. W. Applegate, J. Squier, T. Vestad, J. Oakey, and D. W. M. Marr, "Optical trapping, manipulation, and sorting of cells and colloids in microfluidic systems with diode laser bars," *Opt. Express*, vol. 12, no. 19, pp. 4390–4398, Sep. 2004.
[7] M. P. MacDonald, G. C. Spalding, and K. Dholakia, "Microfluidic sorting in an optical lattice," *Nature*, vol. 426, no. 6965, pp. 421–424, Nov. 2003.
[8] S. L. Neale, M. P. MacDonald, K. Dholakia, and T. F. Krauss, "All-optical control of microfluidic components using form birefringence," *Nat. Mater.*, vol. 4, no. 7, pp. 530–533, Jul. 2005.
[9] Y. Y. Sun, X. C. Yuan, L. S. Ong, J. Bu, S. W. Zhu, and R. Liu, "Large-scale optical traps on a chip for optical sorting," *Appl. Phys. Lett.*, vol. 90, no. 3, Jan. 2007, Art. no. 031107.
[10] X. C. Yuan, S. W. Zhu, J. Bu, Y. Y. Sun, J. Lin, and B. Z. Gao, "Large-angular separation of particles induced by cascaded deflection angles in optical sorting," *Appl. Phys. Lett.*, vol. 93, no. 26, pp. 263901–363903, Dec. 2008.
[11] K. Ladavac, K. Kasza, and D. G. Grier, "Sorting mesoscopic objects with periodic potential landscapes: Optical fractionation," *Phys. Rev. E*, vol. 70, no. 1, Jul. 2004, Art. no. 010901.
[12] F. Nan and Z. Yan, "Sorting metal nanoparticles with dynamic and tunable optical driven forces," *Nano Lett.*, vol. 18, no. 7, pp. 4500–4505, Jul. 2018.
[13] F. Nan and Z. Yan, "Creating multifunctional optofluidic potential wells for nanoparticle manipulation," *Nano Lett.*, vol. 18, no. 11, pp. 7400–7406, Nov. 2018.
[14] S. Kawata and T. Tani, "Optically driven Mie particles in an evanescent field along a channeled waveguide," *Opt. Lett.*, vol. 21, no. 21, pp. 1768–1770, Nov. 1996.

[15] K. Wang, E. Schonbrun, and K. B. Crozier, "Propulsion of gold nanoparticles with surface plasmon polaritons: Evidence of enhanced optical force from near-field coupling between gold particle and gold film," *Nano Lett.*, vol. 9, no. 7, pp. 2623–2629, Jul. 2009.
[16] X. Wang, K. Xiao, C. Min, Q. Zou, Y. Hua, and X. C. Yuan, "Theoretical and experimental study of surface plasmon radiation force on micrometer-sized spheres," *Plasmonics*, vol. 8, no. 2, pp. 637–643, Jun. 2013.
[17] K. Grujic, O. G. Helleso, J. P. Hole, and J. S. Wilkinson, "Sorting of polystyrene microspheres using a Y-branched optical waveguide," *Opt. Express*, vol. 13, no. 1, pp. 1–7, Jan. 2005.
[18] N. K. Grady *et al.*, "Terahertz metamaterials for linear polarization conversion and anomalous refraction," *Science*, vol. 340, no. 6138, pp. 1304–1307, Jun. 2013.
[19] A. V. Kildishev, A. Boltasseva, and V. M. Shalaev, "Planar photonics with metasurfaces," *Science*, vol. 339, no. 6125, Mar. 2013, Art. no. 1232009.
[20] X. Ni, N. K. Emani, A. V. Kildishev, A. Boltasseva, and V. M. Shalaev, "Broadband light bending with plasmonic nanoantennas," *Science*, vol. 335, no. 6067, pp. 427–427, Jan. 2012.
[21] N. Yu *et al.*, "Light propagation with phase discontinuities: Generalized laws of reflection and refraction," *Science*, vol. 334, no. 6054, pp. 333–337, Oct. 2011.
[22] A. Berrier, B. Gompf, L. Fu, T. Weiss, and H. Schweizer, "Optical anisotropies of single-meander plasmonic metasurfaces analyzed by Mueller matrix spectroscopy," *Phys. Rev. B*, vol. 89, no. 19, May 2014, Art. no. 195434.
[23] M. Khorasaninejad, W. T. Chen, R. C. Devlin, J. Oh, A. Y. Zhu, and F. Capasso, "Metalenses at visible wavelengths: Diffraction-limited focusing and subwavelength resolution imaging," *Science*, vol. 352, no. 6290, pp. 1190–1194, Jun. 2016.
[24] Y. Ma, G. Rui, B. Gu, and Y. Cui, "Trapping and manipulation of nanoparticles using multifocal optical vortex metalens," *Sci. Rep.*, vol. 7, no. 1, Nov. 2017, Art. no. 14611.
[25] J. B. Pendry, "Negative refraction makes a perfect lens," *Phys. Rev. Lett.*, vol. 85, no. 18, pp. 3966–3969, Oct. 2000.
[26] J. Hu *et al.*, "All-dielectric metasurface circular dichroism waveplate," *Sci. Rep.*, vol. 7, no. 1, Jan. 2017, Art. no. 41893.
[27] A. Zhu, Q. Qian, Y. Yan, J. Hu, X. Zhao, and C. Wang, "Ultrathin plasmonic quarter waveplate using broken rectangular annular metasurface," *Opt. Laser Technol.*, vol. 92, pp. 120–125, Jul. 2017.
[28] X. Zhao *et al.*, "Electromechanically tunable metasurface transmission waveplate at terahertz frequencies," *Optica*, vol. 5, no. 3, pp. 303–310, Mar. 2018.
[29] J. K. Gansel *et al.*, "Gold helix photonic metamaterial as broadband circular polarizer," *Science*, vol. 325, no. 5947, pp. 1513–1515, Sep. 2009.
[30] Y. Zhao, M. A. Belkin, and A. Alù, "Twisted optical metamaterials for planarized ultrathin broadband circular polarizers," *Nat. Commun.*, vol. 3, no. 1, May 2012, Art. no. 870.
[31] J. Liu, Z. Li, W. Liu, H. Cheng, S. Chen, and J. Tian, "High-efficiency mutual dual-band asymmetric transmission of circularly polarized waves with few-layer anisotropic metasurfaces," *Adv. Opt. Mater.*, vol. 4, no. 12, pp. 2028–2034, Dec. 2016.
[32] H. Kurosawa, B. Choi, Y. Sugimoto, and M. Iwanaga, "High-performance metasurface polarizers with extinction ratios exceeding 12000," *Opt. Express*, vol. 25, no. 4, pp. 4446–4455, Feb. 2017.
[33] K. Meng *et al.*, "Tunable broadband terahertz polarizer using graphene-metal hybrid metasurface," *Opt. Express*, vol. 27, no. 23, pp. 33768–33778, Nov. 2019.
[34] G. Tkachenko, D. Stellinga, A. Ruskuc, M. Chen, K. Dholakia, and T. F. Krauss, "Optical trapping with planar silicon metalenses," *Opt Lett*, vol. 43, no. 14, pp. 3224–3227, Jul. 2018.
[35] X. Wang, Y. Dai, Y. Zhang, C. Min, and X. Yuan, "Plasmonic manipulation of targeted metallic particles by polarization-sensitive metalens," *ACS Photon.*, vol. 5, no. 7, pp. 2945–2950, Jul. 2018.
[36] H. Markovich, I. I. Shishkin, N. Hendler, and P. Ginzburg, "Optical manipulation along an optical axis with a polarization sensitive meta-Lens," *Nano Lett.*, vol. 18, no. 8, pp. 5024–5029, Aug. 2018.
[37] P. Salami and L. Yousefi, "Far-field subwavelength imaging using phase gradient metasurfaces," *J. Lightw. Technol.*, vol. 37, no. 10, pp. 2317–2323, May 2019.
[38] Y. Roichman, B. Sun, Y. Roichman, J. Amato-Grill, and D. G. Grier, "Optical forces arising from phase gradients," *Phys. Rev. Lett.*, vol. 100, no. 1, Jan. 2008, Art. no. 013602.
[39] Z. Yan, M. Sajjan, and N. F. Scherer, "Fabrication of a material assembly of silver nanoparticles using the phase gradients of optical tweezers," *Phys. Rev. Lett.*, vol. 114, no. 14, Apr. 2015, Art. no. 143901.
[40] M. Khorasaninejad *et al.*, "Polarization-insensitive metalenses at visible wavelengths," *Nano Lett.*, vol. 16, no. 11, pp. 7229–7234, Nov. 2016.
[41] A. Arbabi, Y. Horie, A. J. Ball, M. Bagheri, and A. Faraon, "Subwavelength-thick lenses with high numerical apertures and large efficiency based on high-contrast transmitarrays," *Nat. Commun.*, vol. 6, no. 1, May 2015, Art. no. 7069.
[42] M. V. Berry, "The adiabatic phase and Pancharatnam's phase for polarized light," *J. Mod. Optic.*, vol. 34, no. 11, pp. 1401–1407, Nov. 1987.
[43] S. Pancharatnam, "Generalized theory of interference and its applications," *P. Indian AS. - Math. Sci.*, vol. 44, no. 6, pp. 398–417, Dec. 1956.
[44] L. Novotny, R. X. Bian, and X. S. Xie, "Theory of nanometric optical tweezers," *Phys. Rev. Lett.*, vol. 79, no. 4, pp. 645–648, Jul. 1997.
[45] A. H. J. Yang, T. Lerdsuchatawanich, and D. Erickson, "Forces and transport velocities for a particle in a slot waveguide," *Nano Lett.*, vol. 9, no. 3, pp. 1182–1188, Mar. 2009.
[46] X. Chen *et al.*, "Dual-polarity plasmonic metalens for visible light," *Nat. Commun.*, vol. 3, no. 1, Nov. 2012, Art. no. 1198.
[47] K. Svoboda and S. M. Block, "Optical trapping of metallic Rayleigh particles," *Opt. Lett.*, vol. 19, no. 13, pp. 930–932, Jul. 1994.